NASA Technical Memorandum 103980

Coherent Structures in a Simulated Turbulent Mixing Layer

Robert D. Moser and Michael M. Rogers, Ames Research Center, Moffett Field, California

October 1992

National Aeronautics and
Space Administration

Ames Research Center
Moffett Field, California 94035-1000

SUMMARY

A direct numerical simulation of a plane turbulent mixing layer has been performed. The simulation was initialized using two turbulent velocity fields obtained from direct numerical simulation of a turbulent boundary layer at momentum thickness Reynolds number 300 (Spalart 1988). The mixing layer is allowed to evolve long enough for self-similar linear growth to occur, with the visual thickness Reynolds number reaching 14,000.

The simulated flow is examined for evidence of the coherent structures expected in a mixing layer (rollers and rib vortices). Before the onset of self-similar growth, such structures are present, with properties similar to the corresponding laminar or transitional structures. In the self-similar growth regime, however, only the rollers are present with no indication of rib vortices and no indication of conventional pairing. This results in a reduction of mixing and layer growth.

1 INTRODUCTION

Since Brown and Roshko's (1974) discovery of large-scale, apparently two-dimensional, structures in turbulent mixing layers, there has been considerable research aimed at determining the origin, universality, and dynamical significance of these structures (see Ho & Huerre, 1984 for a review). The structures appear to be related to the two-dimensional rollers that form due to the instability of a laminar shear layer, and it has been widely assumed that these turbulent coherent structures will behave in the same way as their pre-transition counterparts. However, it has also been suggested that two-dimensional turbulent rollers are not a universal feature of mixing layers (Chandrsuda *et al.*, 1978), implying that the occurrence of such structures depends on the character of the inlet disturbances, which may be facility dependent.

The assumption that the turbulent rollers are dynamically similar to their nonturbulent counterparts is attractive because much is already known about laminar rollers and their instabilities. In particular, it is known that an array of such rollers is unstable to subharmonic disturbances, which lead to pairing (Kelly 1967, Pierrehumbert & Widnall 1982) and indeed pairings have been reported in turbulent mixing layers. It is also known that the rollers are unstable to three-dimensional disturbances that result in their bending and the formation of the so-called rib vortices in the braid regions between the rollers (Pierrehumbert & Widnall 1982, Corcos & Lin 1984). Recent results (Rogers & Moser 1992) suggest that this three-dimensional instability is governed by two interacting mechanisms, one characteristic of flows dominated by rotation (as in the roller), which leads to the bending of the roller, and the other associated with strain-dominated flows (as in the braid or saddle region), which leads to the formation of the rib vortices. As pointed out by Rogers & Moser (1992), the magnitude of the strain in the braids and rollers of the two-dimensional rolled up mixing layer is about the same at the center line, so the difference in character between the two regions is caused by the reduced levels of spanwise vorticity in the braid region. Thus, if the turbulent rollers lead to braid regions that are substantially depleted of spanwise vorticity, we might expect rib vortices to form in the turbulent flow as well. There is experimental evidence for rib vortices in turbulent mixing layers (*e.g.* Breidenthal 1981, Jimenez 1983, Bernal & Roshko 1986). However, it is not clear under what circumstances the laminar stability ideas discussed above are applicable to turbulent mixing layers.

To address the issues raised above, a direct numerical simulation of a turbulent mixing layer was performed. The simulation was designed to model an experimental situation in which the splitter plate boundary layers are turbulent and no external perturbations are present. The resulting flow fields are

examined for evidence of the large scale rollers and other flow features that are expected by analogy with the structure in nonturbulent flows (*i.e.* spanwise rollers and streamwise rib vortices). In what follows, §2 is a description of the simulation, §3 is a discussion of the large scale rollers and their pairing, and §4 contains a description of the three-dimensional structure. Discussion and concluding remarks are given in §5.

2 THE SIMULATION

The numerical simulation discussed in this paper was performed by solving the three-dimensional time-dependent incompressible Navier-Stokes equations. For computational efficiency, a temporally evolving mixing layer was simulated rather than the spatially evolving layer typical of experiments. Comparisons of direct numerical simulations show that the temporally and spatially evolving mixing layers are qualitatively and quantitatively similar (Buell, Moser & Rogers 1992). In this study, the solution domain is periodic in the streamwise (x) and spanwise (z) directions with periods $125\delta_m^0$ and $31.25\delta_m^0$ respectively, where δ_m^0 is the initial momentum thickness of the layer. The domain is infinite in the cross-stream (y) direction. A Galerkin spectral method (Spalart, Moser & Rogers 1991) was used to solve the equations. A passive scalar with Schmidt number 1.0 that goes to zero and one in the free streams, is also simulated.

Initial conditions were generated using two realizations of a turbulent boundary layer with a momentum thickness Reynolds number of 300, as computed by Spalart (1988). One boundary layer was used for each side of the mixing layer, with equal and opposite free stream velocities attained at $y = \pm\infty$. The resulting initial mixing layer profile had a Reynolds number of 800 based on the velocity difference across the layer (ΔU) and the momentum thickness, δ_m, defined as

$$\delta_m = \int_{-\infty}^{\infty} \frac{1}{4} - U^2 \, dy,$$

where U is the mean velocity normalized by ΔU. In the remainder of the paper ΔU and the initial momentum thickness δ_m^0 are used to nondimensionalize all quantities, unless otherwise noted.

The flow was allowed to evolve for a total time of 187.5, at which time the momentum thickness had grown by a factor or three. As can be seen in figure 1, the momentum thickness begins growing linearly, which is characteristic of self-similar evolution, at $t \approx 70$. Also, the integrated (in y) turbulent kinetic energy density q_i^2 grows linearly and the integrated dissipation rate ϵ_i is approximately constant by $t \approx 120$. These are the expected behaviors for a self-similar mixing layer. The self-similar growth rate $d\delta_m/dt$ (normalized by ΔU) in the simulation is 0.014, which is in fairly good agreement with the value of 0.016 found in the experiments of Hussain & Zaman (1985). The discrepancy with the value of 0.02 found by Brown & Roshko (1974) and Rodi(1975) is larger. These observations provide evidence that the simulation represents a self-similar turbulent mixing layer for $t > 120$.

At $t = 120$, when the layer becomes self-similar, the momentum thickness of the simulated layer has only grown by a factor of 2, which is small compared to the growth required to attain self-similarity in many experiments (*e.g.* a factor of about 10 in Hussain & Zaman, 1985 and a factor of about 9 in Mehta & Westphal 1985). There are two likely explanations for this difference. First, the inlet mean velocity profiles are different in the experiments and the computations. The experimental profiles, being asymmetric, may require more development to become self-similar. Second, the experiments may inadvertently include

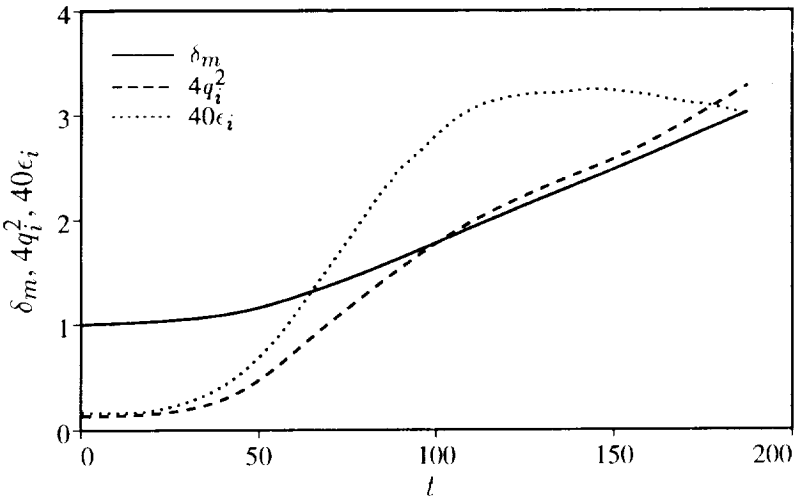

Figure 1. Evolution of momentum thickness (δ_m), integrated (in y) kinetic energy density (q_i^2), and integrated dissipation rate (ϵ_i).

organized disturbances (*e.g.* two-dimensional disturbances resulting from the receptivity of the splitter-plate tip). It may take a long development for the effects of these disturbances to be eliminated. It is also not clear if the effects of such disturbances would extend into the self-similar regime.

In the following sections, the simulated mixing layer is examined for coherent structures at two times, one in the self-similar regime ($t = 187.5$) and one prior to the self-similar regime ($t = 78.5$). The earlier time is late enough for mixing-layer structures to have formed from the initial turbulent boundary layers, but is before the layer has reached self-similarity.

3 SPANWISE ROLLERS AND PAIRING

Contours of spanwise vorticity (ω_z) in an x–y plane of the mixing layer (figure 2) show that at both times examined ($t = 78.5$ and 187.5) there are amalgamations of spanwise vorticity (rollers) interspersed with thinner regions that have less spanwise vorticity (braids). At the later time, the braid regions still contain many small-scale vorticity fluctuations. However, at the earlier time there are at least some braid regions that are nearly devoid of spanwise vorticity. These "clean" braids are similar to those found in laminar and transitional mixing layers (*e.g.* Rogers & Moser 1992, Lasheras, Cho & Maxworthy, 1986), and to those found in some flow visualizations of turbulent layers (*e.g.* Brown & Roshko 1974).

To study the large-scale structures in more detail, a diagnostic that will locate the rollers and braid regions in x and z is needed. This is similar to the situation in experiments, where a structure must be detected so that it can be included in an ensemble average of similar structures. In this case, however, we wish to map the location and size of the structures in space; no averaging is to be done. The results of Rogers & Moser (1992) suggest that the most important difference between the braids and rollers is the strain dominance of the former and the rotation dominance of the latter. To this end, we consider the two quantities:

$$\Omega = -\frac{1}{2}\int_{-\infty}^{\infty} \omega_z \, dy \quad \text{and} \quad \Sigma_{ij} = \int_{-\infty}^{\infty} S_{ij} \, dy,$$

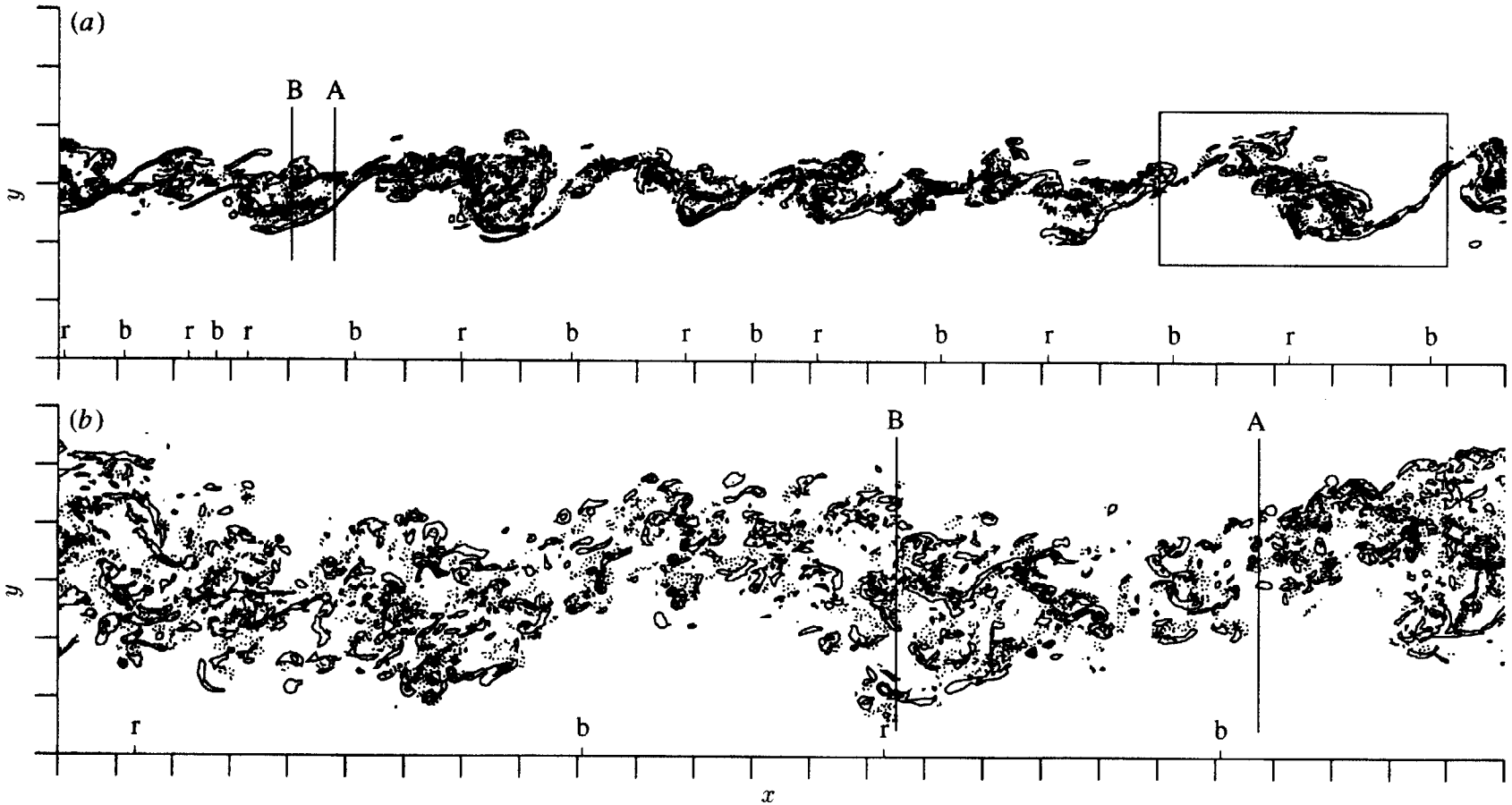

Figure 2. Contours of spanwise vorticity in x–y planes at (a) $z = 18.8$ and $t = 78.5$, (b) $z = 0$ and $t = 187.5$. Contour increments are ± 0.25, positive contours are dotted, and tic marks are at $5\delta_m^0$ increments. Locations marked "b" and "r" are the centers of the braids and rollers respectively as determined from the V diagnostic (see text). The vertical lines mark the locations of the z–y planes depicted in figures 5 and 6. The evolution of the region marked by the box in (a) is shown in figure 4.

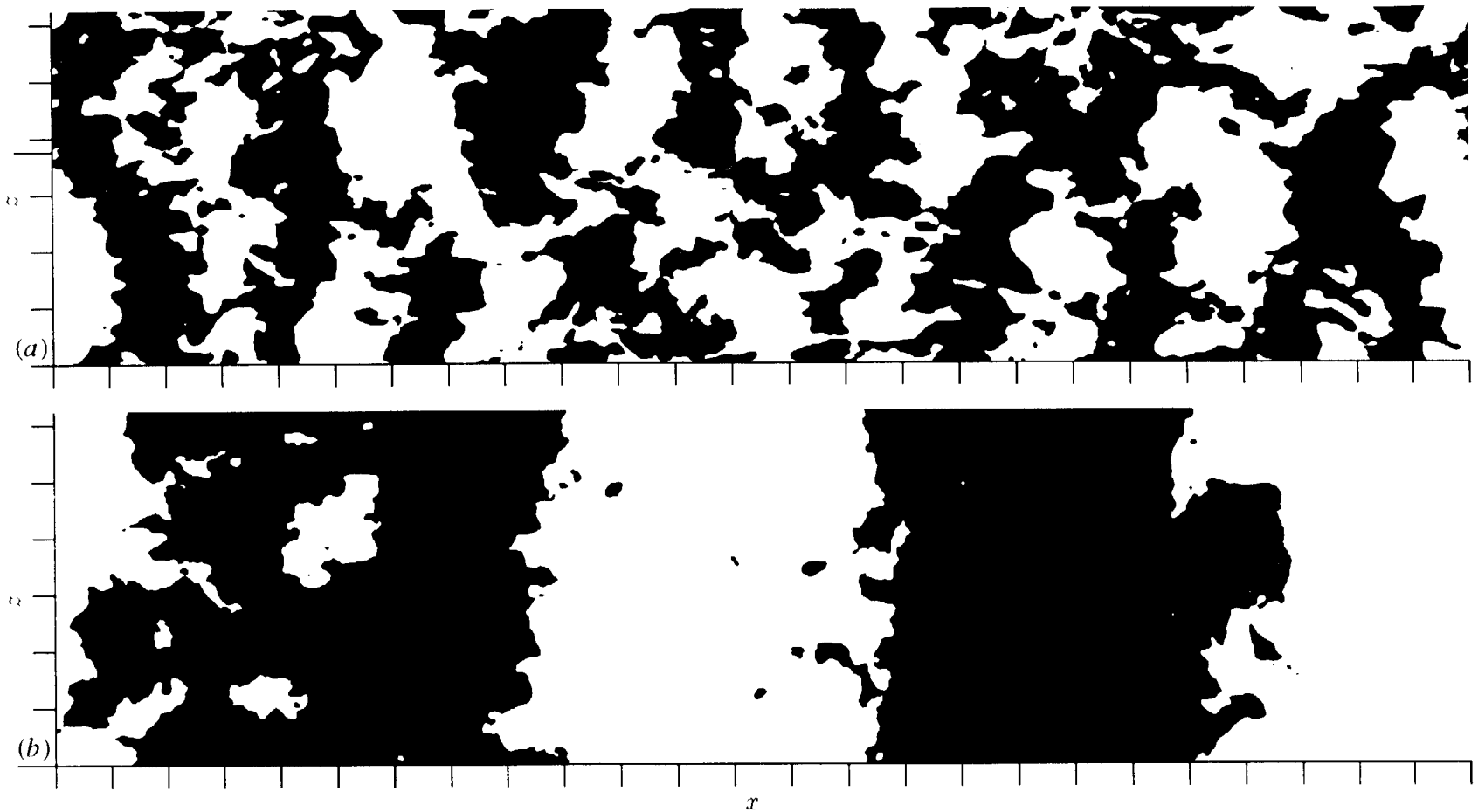

Figure 3. Locations in x and z where $V = \int_{-\infty}^{\infty} v\,dy < 0$ (shown in black) at (a) $t = 78.5$ and (b) $t = 187.5$. Braid regions are located at boundaries with black to the left, rollers are located at boundaries with black to the right. Tic marks are at $5\delta_m^0$ intervals and the extra long tic marks on the z axes indicate the z location of the planes shown in figures 2 and 4.

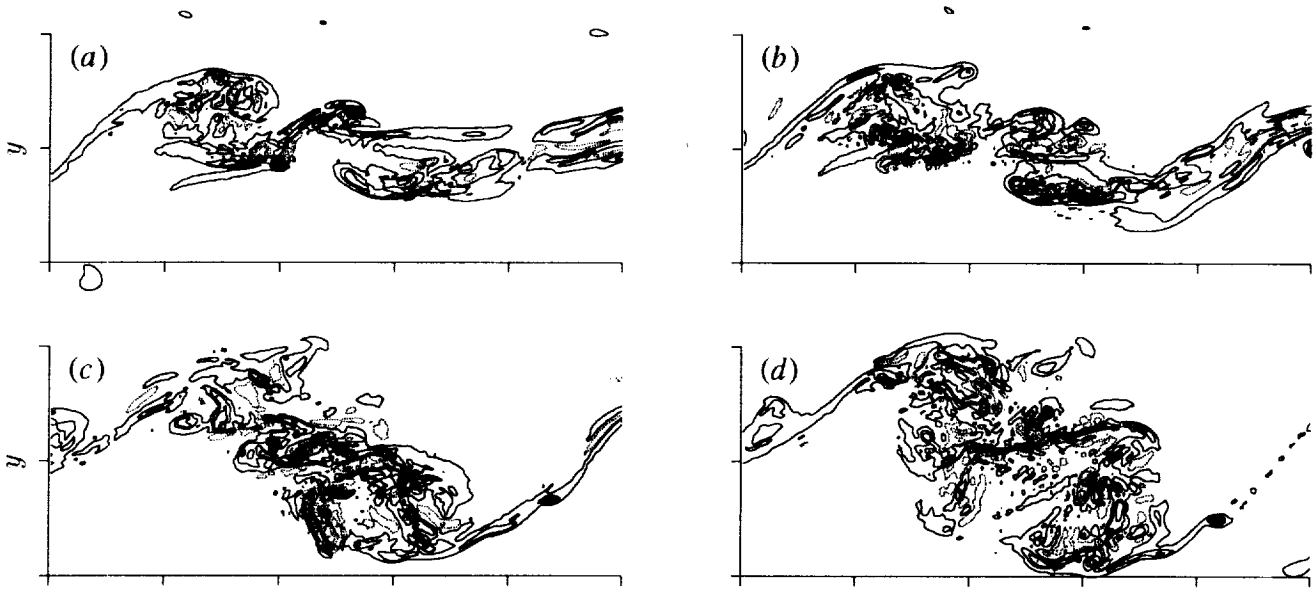

Figure 4. Contours of spanwise vorticity in the $z = 18.8$ x–y plane at (a) $t = 59.4$, (b) $t = 66.3$, (c) $t = 78.5$, and (d) $t = 85.9$. The domain depicted is marked with a box in figure 2(a). The contour increment is ± 0.4, positive contours are dotted, and tic marks are at $5\delta_m^0$ intervals.

where S_{ij} is the strain-rate tensor, and the cross-stream integral eliminates some of the contributions of small-scale features. When normalized by the local thickness, these quantities are measures of the large-scale vorticity and strain-rate tensor. The layer may be said to be strain dominated where the principal value of Σ_{ij} in the plane normal to the mean vorticity is greater than Ω. This condition reduces to

$$\frac{\partial V}{\partial x} = \frac{\partial}{\partial x} \int_{-\infty}^{\infty} v \, dy > 0.$$

It is expected that $\partial V/\partial x$ will be negative where there are rollers and will be positive where there are braids, and indeed this is the case for the flow considered here. However, variations in $\partial V/\partial x$ are still dominated by small scales, so we consider V instead, which will be decreasing with x in the rollers and increasing with x in the braids. A plot showing where (in x and z) V is positive and negative shows the rollers and braids. In figure 3, braids are seen as boundaries between white and black where black is on the left. A variety of other diagnostics have been tried (*e.g.* integrated in y enstrophy, scalar thickness, integrated strain-rate), but they were all overly sensitive to small-scale features.

The V diagnostic suggests that there are rollers and braid regions in the flow at both times, in agreement with the contour plots in figure 2. The centers of the braids and rollers as determined from V in the planes depicted are marked in figure 2. The V diagnostic also gives an indication of the spanwise coherence of the structures. At $t = 78.5$, the structures have a spanwise extent as large as the streamwise spacing, or larger, but they do not span the entire spanwise domain. There are 8 or 9 rollers in streamwise domain shown. In contrast, the structures at $t = 187.5$ *do* span the domain in z and there are only two structures in x. Since the spanwise domain size is smaller than the streamwise spacing of the structures at $t = 187.5$, it is not possible for the rollers to have the spanwise variations present at the earlier time. Thus the two-dimensionality of the rollers at this time is an artifact of the computation. Remarkably, the number of structures in the streamwise direction has decreased by a factor of about 4 between the times

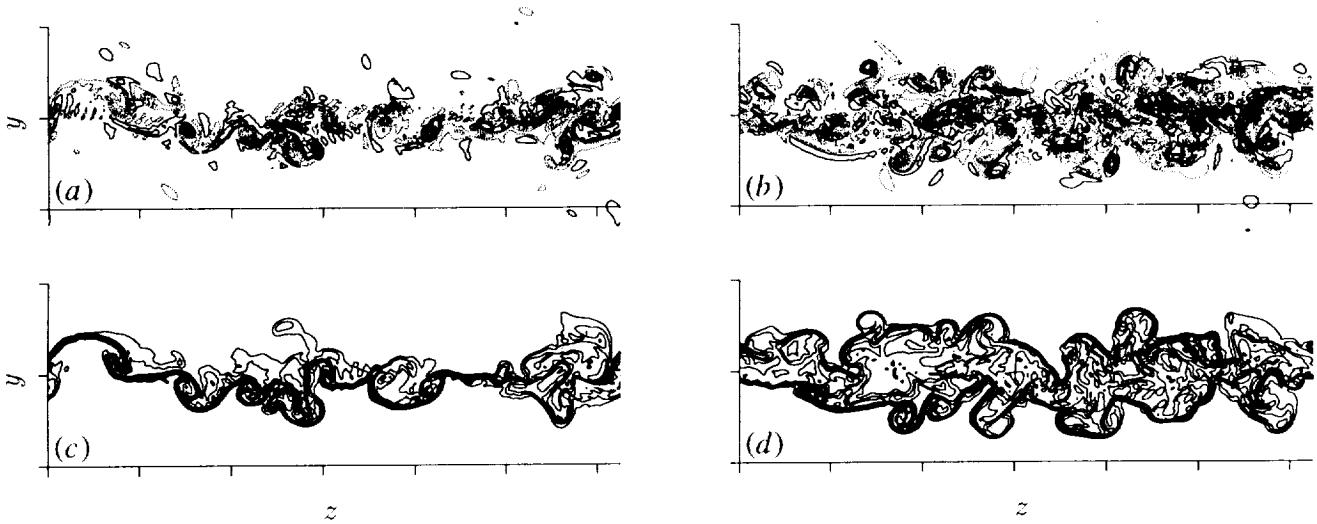

Figure 5. Contours of (a,b) streamwise vorticity and (c,d) passive scalar in the z–y plane at the line marked (a,c) A (braid region) and (b,d) B (roller) in figure 2(a) at $t = 78.5$. The contour increment is (a,b) 0.3, (c,d) 0.1, positive contours are dotted, and tic marks are at $5\delta_m^0$ intervals.

depicted, while the momentum thickness has only increased by a factor of 2. This is consistent with the fact that the rollers appear more elongated at $t = 187.5$ (figure 2(b)).

The roller structures in this flow have clearly increased their streamwise length scale, so one wonders if they did so by the pairing mechanism associated with laminar rolled-up mixing layers. At the earlier time (before self-similarity), pairing apparently does occur. The two rollers in the box in figure 2(a) are rotating one above the other, as can be seen in figure 4. However, after self-similarity no such pairings have been detected. When the self-similar structures change scale, the vorticity from one roller appears to ooze gradually into its neighbors, without the co-rotation characteristic of pairing. This may be the reason why Hussain & Zaman (1985) were unable to detect pairings in their self-similar turbulent mixing layer.

4 RIB VORTICES

In laminar and transitional mixing layers, the dynamics of the braid region and those of the roller are different due to the strain dominance of the former and the rotation dominance of the latter (Rogers & Moser 1992). In particular, the braid region is apparently susceptible to a three-dimensional instability, resulting in the formation of streamwise rib vortices. If coherent rib vortices are present in the turbulent flow, they should be relatively easy to detect. In contrast, three-dimensional instabilities of the roller lead to a bending of the roller, which would be difficult to detect in a turbulent flow. We will thus examine the simulated flow at $t = 78.5$ and $t = 187.5$ for evidence of rib vortices.

Contours of streamwise vorticity and the passive scalar in the braid regions (z–y planes marked by the vertical lines labeled "A" in figure 2) and rollers (plane marked "B" in figure 2) are shown for both times in figures 5 and 6. These rollers and braids were selected because they are the most spanwise coherent (see figure 3). At $t = 78.5$, the strong streamwise vorticity in this plane is dominated by compact approximately circular regions of intense vorticity. The passive scalar contours indicate a sharp interface in the scalar, and this interface is rolled up around the streamwise vortices. These features are characteristic of ribs in the

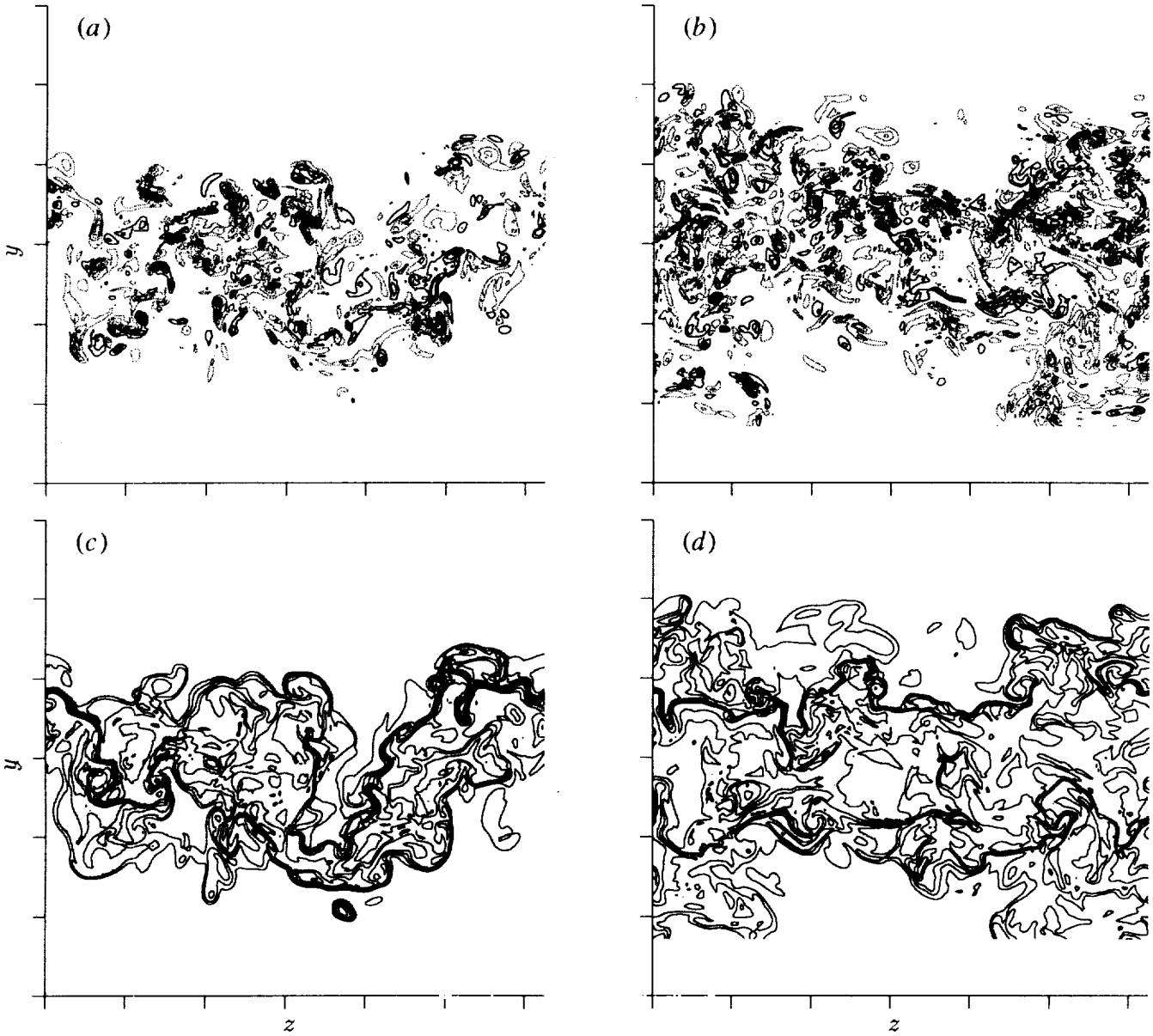

Figure 6. Contours of (*a,b*) streamwise vorticity and (*c,d*) passive scalar in the z–y plane at the line marked (*a,c*) A (braid region) and (*b,d*) B (roller) in figure 2(*b*) at $t = 187.5$. The contour increment is (*a,b*) 0.3, (*c,d*) 0.1, positive contours are dotted, and tic marks are at $5\delta_m^0$ intervals.

braid regions of nonturbulent mixing layers. In contrast, the streamwise vorticity at $t = 187.5$ (figure 6) is not well organized, although there are a few small circular regions of intense vorticity. The scalar at this time does not have the single sharp interface with discrete rollups seen at the earlier time. Comparing the braid region (figure 6(*a*)) to the roller core (figure 6(*b*)) suggests that at $t = 187.5$ the major difference between the braid and roller is that the vortical region in the braid is thinner in the y direction.

A top view of the high-enstrophy regions of the mixing layer at the two times is shown in figure 7. At $t = 78.5$, many of the braid regions are visible as (white) regions with relatively little vorticity (compare to figure 3). In this figure, the ribs are the long thin roughly streamwise vortices spanning many of the

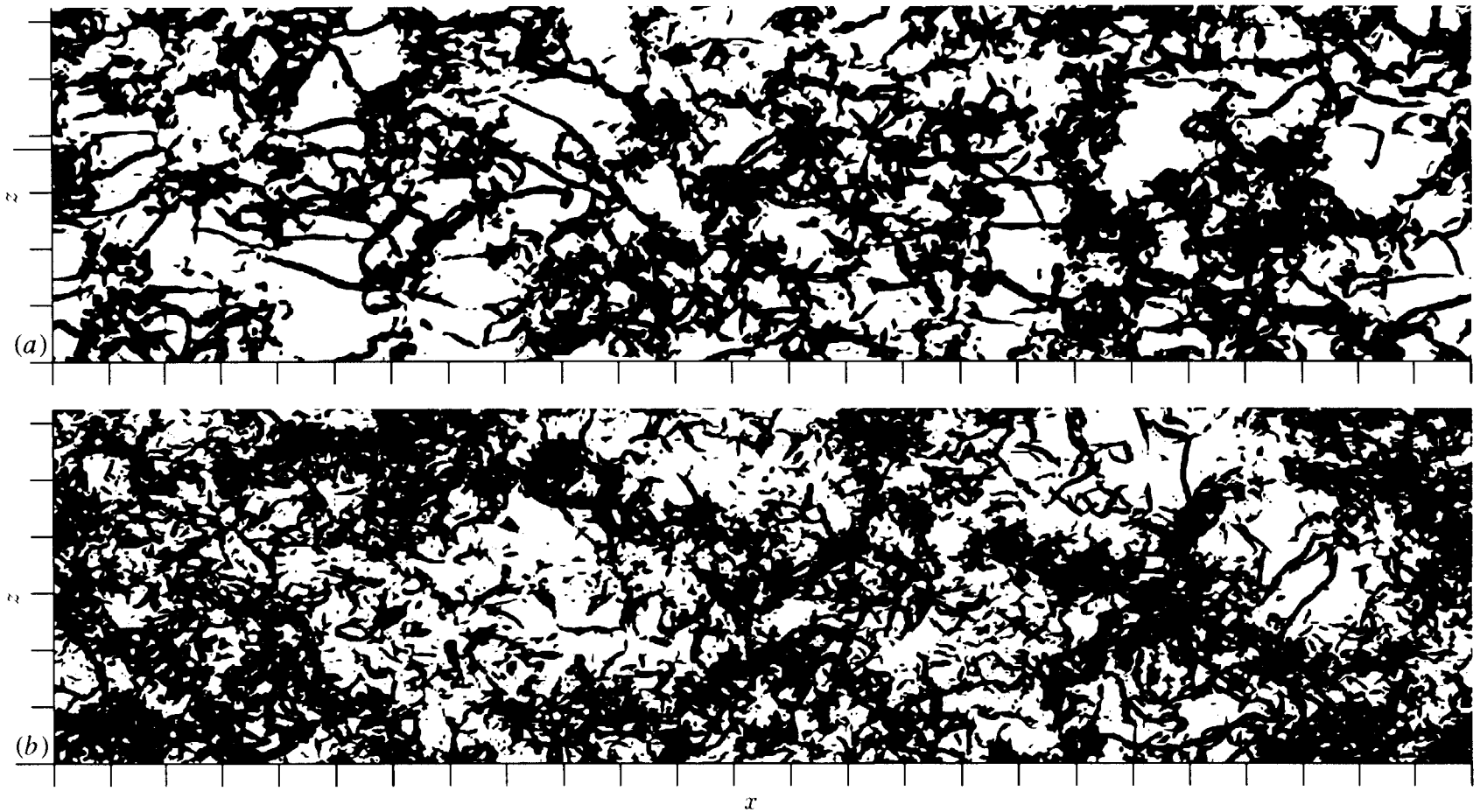

Figure 7. Plan view of high-enstrophy structures (enstrophy greater than (*a*) 2.6, (*b*) 2.0) at (*a*) $t = 78.5$ and (*b*) $t = 187.5$. Tic marks are at $5\delta_m^0$ intervals and the extra long tic marks on the z axes indicate the z location of the planes shown in figures 2 and 4.

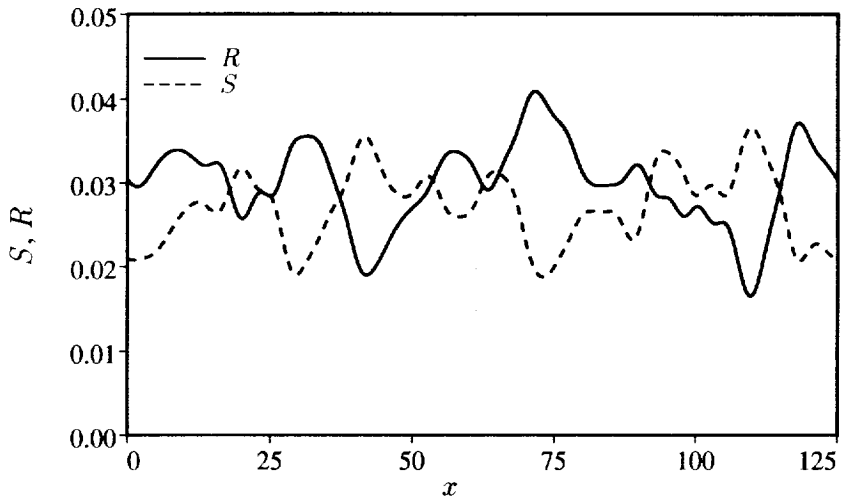

Figure 8. Streamwise (x) variation of the average principal two-dimensional strain rate (S) and average rotation rate ($R = -\omega_z/2$) at $t = 187.5$. The average is taken over the spanwise direction, over the vertical direction in the vortical region ($|\omega_z| > 0.04$), and in the streamwise direction using a Gaussian filter of width 5.

braid regions. At $t = 187.5$, however, the braid regions are not clearly visible, though there is some tendency for the vorticity to be denser in the rollers. Rib vortices are also not so obvious at this time. Although there are some small-scale vortices visible in this figure, none of them extends across an entire braid region. In addition, there does not appear to be any preference for these vortices to occur in the braid region. The small-scale vortices at this time appear to be the "worms" that have been found to be a common feature of turbulent flows (Jimenez, 1992). Jimenez has suggested that turbulent flows have worm vortices with circulation Reynolds numbers (Γ/ν) between 200 and 400. Estimates of the circulations of the strong vortices in figure 6(a) are of this order. However, estimates of rib-vortex circulations in the flow at $t = 78.5$ (figure 5(a)) are as much as 800, suggesting that these vortices represent more than just small-scale turbulent structure.

While the structure of the turbulence in the braids and rollers appears to be similar at $t = 187.5$, the large-scale deformation imposed on the turbulence is different in the two regions. This can be quantified by computing average rotation and strain rates in different regions of the mixing layer. At $t = 187.5$, the rollers are mostly two-dimensional (see figure 3), so a spanwise average can be used. In addition, averages were taken in across the vortical region in y (the region where the magnitude of span averaged ω_z is greater than 0.04) and locally in x (using a Gaussian filter with a width of 5). The resulting average two-dimensional principal strain rate and rotation rate ($-\omega_z/2$) are shown as a function of x in figure 8. As expected, the braid regions are strain dominated with strain rates as much as twice the rotation rates, while the rollers are rotation dominated, also by as much as a factor of two. One might expect the effects of this difference to be similar to the effects of such mixed strains on homogeneous turbulence (*i.e.* intermediate between plain strain and shear in the braids and intermediate between pure rotation and shear in the rollers). However, homogeneous turbulence subjected to such strains has not been thoroughly investigated. In any case, the differences between the turbulence in the braids and rollers are clearly too subtle to be detected by the crude visual diagnostics used in figures 6 and 7.

5 DISCUSSION AND CONCLUSIONS

The observations presented above show that there is a fundamental difference between the large-scale structures in a self-similar turbulent mixing layer and the large-scale structures in the same layer before self-similarity is achieved. Prior to selfsimilarity, the structures correspond closely to the transitional structures that have been studied extensively (Rogers & Moser 1992, Moser & Rogers 1993, and others), with rollers that pair and rib vortices spanning the braid regions. There is no such correspondence in the self-similar regime, which has neither pairings nor rib vortices. It appears that the turbulence in the braid region is not qualitatively different from that in the roller.

Since the "rollers" in this self-similar turbulent mixing layer do not appear to have the dynamical properties expected of such structures, it is not clear what relevance they have to the global development of the mixing layer. For example, if the rollers do not pair, then they will not entrain large amounts of free-stream fluid the way nonturbulent rollers do. Thus, they will not be responsible for a large portion of the mixing layer growth, nor will they dominate the mixing process as was assumed by Broadwell & Breidenthal (1982) in developing their mixing model. The only dynamical significance of the roller structures appears to be that they set the deformation environment in which the turbulence evolves, creating strain-dominated and rotation-dominated regions. The effects of this on the turbulence are yet to be determined.

The lack of ribs and pairings in our self-similar flow is different from several experiments (*e.g.* Brown & Roshko 1974, Konrad 1976, Breidenthal 1980, Jimenez 1983) in which measurements show the layer to be self-similar while flow visualization suggests that ribs and pairings are present. A possible explanation for this difference is the disturbance environment in the experiments, which may include much stronger two-dimensional or quasi-two-dimensional disturbances than are present in the current simulations. Such disturbances might arise due to the receptivity of the splitter-plate tip (Ho & Huerre 1984). The experimental disturbances may also include strong streamwise vortices from imperfections in the facility upstream of the splitter plate tip as in Jimenez (1983). The presence of strong two-dimensional disturbances may also explain the somewhat higher self-similar growth rate in the experiments, because organized pairings of two-dimensional rollers would promote spreading of the layer.

REFERENCES

BERNAL, L. P. & ROSHKO, A. 1986 Streamwise vortex structure in plane mixing layers. *J. Fluid Mech.* **170,** 499–525.

BREIDENTHAL, R. 1981 Structure in turbulent mixing layers and wakes using a chemical reaction. *J. Fluid Mech.* **109,** 1–24.

BROADWELL, E. J. & BREIDENTHAL, R. E. 1982 A simple model of mixing and chemical reaction in a turbulent shear layer. *J. Fluid Mech.* **125,** 397-410.

BROWN, G. L. & ROSHKO, A. 1974 On density effects and large structure in turbulent mixing layers. *J. Fluid Mech.* **64,** 775–816.

BUELL, J. C., MOSER, R. D. & ROGERS, M. M. 1992 A comparison of spatially and temporally developing mixing layers. *in preparation*

CHANDRSUDA, C., MEHTA, R. D., WEIR, A. D. & BRADSHAW, P. 1978 Effect of free-stream turbulence on large structure in turbulent mixing layers. *J. Fluid Mech.* **85,** 693–704.

CORCOS, G. M. & LIN, S. J. 1984 The mixing layer: deterministic models of a turbulent flow. Part 2. The origin of the three-dimensional motion. *J. Fluid Mech.* **139,** 67–95.

HO, C.-M. & HUERRE, P. 1984 Perturbed free shear layers. *Ann. Rev. Fluid Mech.* **16,** 365–424.

HUSSAIN, A. K. M. F. & ZAMAN, K. M. B. Q. 1985 An experimental study of organized motions in the turbulent plane mixing layer. *J. Fluid. Mech.* **159,** 85–104.

JIMENEZ, J. 1983 A spanwise structure in the plane shear layer. *J. Fluid Mech.* **132,** 319–336.

JIMENEZ, J. 1992 Kinematic alignment effects in turbulent flows. *Phys. Fluids A.* **4,** 652-654.

KELLY, R. E. 1967 On the stability of an inviscid shear layer which is periodic in space and time. *J. Fluid Mech.* **27,** 657–689.

KONRAD, J. H. 1976 An experimental investigation of mixing in two-dimensional turbulent shear flows with applications to diffusion-limited chemical reactions. *Intern. Rep.* CIT-8-PU, Calif. Inst. Technol. Pasadena, CA.

LASHERAS, J. C., CHO, J. S. & MAXWORTHY, T. 1986 On the origin and evolution of streamwise vortical structures in a plane, free shear layer. *J. Fluid Mech.* **172,** 231–258.

MEHTA, R. D. & WESTPHAL, R. V. 1985 An experimental study of plane mixing layer development. *NASA TM86698.*

MOSER, R. D. & ROGERS, M. M. 1993 The three-dimensional evolution of a plane mixing layer: pairing and transition to turbulence. *J. Fluid. Mech.* to appear.

PIERREHUMBERT, R. T. & WIDNALL, S. E. 1982 The two- and three-dimensional instabilities of a spatially periodic shear layer. *J. Fluid Mech.* **114,** 59–82.

RODI, W. 1975 A review of experimental data of uniform density free turbulent boundary layers. in *Studies in Convection.* **1,** B. E. Launder, ed., Academic Press, 79-165.

ROGERS, M. M. & MOSER, R. D. 1992 The three-dimensional evolution of a plane mixing layer: The Kelvin–Helmholtz rollup. *J. Fluid. Mech.* **243,** 183-226.

SPALART, P. R. 1988 Direct simulation of a turbulent boundary layer up to $R_\theta = 1410$. *J. Fluid Mech.* **187,** 61-98.

SPALART, P. R., MOSER, R. D. & ROGERS, M. M. 1991 Spectral methods for the Navier–Stokes equations with one infinite and two periodic directions. *J. Comp. Phys.* **96,** 297–324.

REPORT DOCUMENTATION PAGE

Form Approved
OMB No. 0704-0188

1. AGENCY USE ONLY *(Leave blank)*	2. REPORT DATE	3. REPORT TYPE AND DATES COVERED
	October 1992	Technical Memorandum

4. TITLE AND SUBTITLE

Coherent Structures in a Simulated Turbulent Mixing Layer

5. FUNDING NUMBERS

505-59-53

6. AUTHOR(S)

Robert D. Moser and Michael M. Rogers

7. PERFORMING ORGANIZATION NAME(S) AND ADDRESS(ES)

Ames Research Center
Moffett Field, CA 94035-1000

8. PERFORMING ORGANIZATION REPORT NUMBER

A-92197

9. SPONSORING/MONITORING AGENCY NAME(S) AND ADDRESS(ES)

National Aeronautics and Space Administration
Washington, DC 20546-0001

10. SPONSORING/MONITORING AGENCY REPORT NUMBER

NASA TM-103980

11. SUPPLEMENTARY NOTES

Point of Contact: Robert D. Moser, Ames Research Center, MS 202A-1, Moffett Field, CA 94035-1000
(415) 604-4733

12a. DISTRIBUTION/AVAILABILITY STATEMENT

Unclassified-Unlimited
Subject Category – 34

12b. DISTRIBUTION CODE

13. ABSTRACT ***(Maximum 200 words)***

A direct numerical simulation of a plane turbulent mixing layer has been performed. The simulation was initialized using two turbulent velocity fields obtained from direct numerical simulation of a turbulent boundary layer at momentum thickness Reynolds number 300 (Spalart, 1988). The mixing layer is allowed to evolve long enough for self-similar linear growth to occur, with the visual thickness Reynolds number reaching 14,000.

The simulated flow is examined for evidence of the coherent structures expected in a mixing layer (rollers and rib vortices). Before the onset of self-similar growth, such structures are present with properties similar to the corresponding laminar or transitional structures. In the self-similar growth regime, however, only the rollers are present with no indication of rib vortices and no indication of conventional pairing. This results in a reduction of mixing and layer growth.

14. SUBJECT TERMS	15. NUMBER OF PAGES
Turbulence, Mixing layer, Coherent structures	17
	16. PRICE CODE: A02

17. SECURITY CLASSIFICATION OF REPORT	18. SECURITY CLASSIFICATION OF THIS PAGE	19. SECURITY CLASSIFICATION OF ABSTRACT	20. LIMITATION OF ABSTRACT
Unclassified	Unclassified		